Journal of Materials Chemistry A

A Highly Active and Cr-Resistant Infiltrated Cathode for Practical Solid Oxide Fuel Cells

Journal:	*Journal of Materials Chemistry A*
Manuscript ID	TA-COM-10-2019-011657.R1
Article Type:	Communication
Date Submitted by the Author:	25-Nov-2019
Complete List of Authors:	Huang, Kevin; University of South Carolina yang, tianrang; Northwestern University, Wen, Yeting; University of South Carolina System Wu, Tao; University of South Carolina, Xu, Nansheng; University of South Carolina

Communication

A Highly Active and Cr-Resistant Infiltrated Cathode for Practical Solid Oxide Fuel Cells

Received 00th January 2019,
Accepted 00th January 2019

DOI: 10.1039/x0xx00000x

Tianrang Yang,[ab†] Yeting Wen, [b†] Tao Wu,[b] Nansheng Xu[b] and Kevin Huang [b*]

ABSTRACT: A critical obstacle to the commercialization of modern solid oxide fuel cells (SOFCs) loaded with metallic interconnects is the unacceptable degradation rate resulting from Cr (an element richly present in metallic interconnects) volatilization and its subsequent reaction with the cathode, forming insulating $SrCrO_4$ that blocks oxygen reduction reaction (ORR) active sites. Here we report a Cr-tolerant, yet ORR-active, cathode for sustainable operation of solid oxide fuel cells (SOFCs). The new resilient cathode consists of a continuous, nanoscaled, ORR-active $SrCo_{0.9}Ta_{0.1}O_{3-\delta}$ (SCT) as the capping layer and a commercial $(La_{0.6}Sr_{0.4})_{0.95}Co_{0.2}Fe_{0.8}O_{3-\delta}$ (LSCF)-$Ce_{0.8}Gd_{0.2}O_{1.9}$ (GDC) composite as the underlying skeleton. Stability testing in a high-Cr-content environment shows that the cathode has a remarkable resistance to Cr-attack while retaining superior ORR activity. A successful implantation of this bilayer cathode into practical SOFC stacks will advance the commercialization of SOFC technology.

Developing active and robust intermediate-temperature electrode materials to lower cost and improve reliability for solid oxide fuel cells (SOFCs) has been a major research effort in SOFC commercialization in recent decades. Compared to the fuel oxidation reaction (FOR) at the Ni-based anode, the oxygen reduction reaction (ORR) at the cathode is the performance limiting step in SOFCs.[1,2] Many cathode materials developed so far are oxides with perovskite or related structures, examples of which include $(Sm,Sr)CoO_{3-\delta}$, $(Ba,Sr)(Co,Fe)O_{3-\delta}$ and $(La,Sr)(Co,Fe)O_{3-\delta}$, just to name a few.[3-5] In these perovskite-structured cathodes, Sr is often used as a primary dopant to increase the material's electronic/oxide-ion conductivities for enhanced ORR activity.

One critical issue with these Sr-doped perovskites (SDPs) is the surface Sr-segregation driven by the electrostatic attraction between the Sr-dopant (Sr'_{La}) in the lattice and oxygen vacancies ($V_{\ddot{O}}$) on the surface.[6,7] The resultant free SrO on the surface is widely deemed a leading cause for the performance degradation observed in SOFC stacks due to the thermodynamically favorable reaction between SrO and gaseous hexavalent Cr-species; the latter is a product of the oxidation of Cr in Cr-containing metallic interconnects, a phenomenon also known as "Cr-poisoning".[8,9] Therefore, developing Cr-tolerant cathodes and/or methods to remove gaseous Cr-species from air stream have received much attention in recent years by industrial SOFC developers and academic researchers. Some early studies have shown that some oxides, e.g. $La(NiFe)O_{3-\delta}$ (LNF) and $La_{0.6}Ba_{0.4}Co_{0.2}Fe_{0.8}O_{3-\delta}$ (LBCF), are somewhat Cr-resistant, but either insufficiently ORR active or chemically/thermally unstable.[10-12] Use of a "Cr-getter" such as BaO, $SrMnO_3$, SrO, $Sr_xNi_yO_z$ or $(LaSr)CoO_3$ to capture the gaseous Cr-species is

[a]*Department of Mechanical Engineering, University of South Carolina, Columbia, SC 29208, USA*
[b]*Department of Materials Science and Engineering, Northwestern University, Evanston, IL, 60208, USA*
Email: huang46@cec.sc.edu
Electronic Supplementary Information (ESI) available: Experimental and computational methods; SEM image of SCT@LSCF at 800 °C; Impedance spectra with the presence of Cr; Single cell performance; R_p in Cr-containing atmosphere; Impedance spectra under CO_2 and H_2O containing air; The cathodes morphology and Sr-3d XPS spectra in symmetrical cells post- and pre-annealing at 700 °C; Raman spectra of LSCF pellet after annealing in Cr-containing air. See DOI: 10.1039/x0xx00000x
†These authors contributed equally.

effective, but generally deemed a temporary solution due to its consumable and irreplaceable nature in SOFC stacks.[13-16]

$SrCo_{0.9}Ta_{0.1}O_{3-\delta}$ (SCT) has been reported with comparable electronic conductivity, much higher oxygen diffusion coefficient, surface exchange rate, as well as much better ORR activity and durability than $(La_{0.6}Sr_{0.4})_{0.95}Co_{0.2}Fe_{0.8}O_{3-\delta}$ (LSCF).[17,18] However, SCT by itself is not a practical cathode due to its exceptionally larger thermal expansion than those commonly used electrolytes.[18] We here report on a new Cr-tolerant, stable and ORR-active cathode suitable for practical SOFCs. The new cathode consists of a continuous, nanoscaled $SrCo_{0.9}Ta_{0.1}O_{3-\delta}$ (SCT) capping layer made from solution infiltration over a prefabricated porous $(La_{0.6}Sr_{0.4})_{0.95}Co_{0.2}Fe_{0.8}O_{3-\delta}$ (LSCF)-$Ce_{0.8}Gd_{0.2}O_{1.9}$ (GDC) composite skeleton. In such a structure, the ORR takes place mainly at the surface of SCT, while the porous LSCF-GDC skeleton provides multiple pathways for electronic/ionic conduction and gas transport. We also demonstrate strong experimental and theoretical evidences that support the multifunctionality of the infiltrated cathode.

The phase and morphology of the SCT capping layer are critically important to the performance of the new infiltrated cathode. **Figure 1 (a)** shows that the onset temperature to form a pure perovskite SCT phase is 1000 °C. At this temperature, the morphology of the resultant bilayer cathode (collectively denoted as SCT@LSCF-GDC throughout this paper), shown in **Figure 1 (b)**, exhibits a continuous SCT layer that is intimately bonded to the LSCF-GDC skeleton. This observation is uniquely different from conventional discrete nanoparticles (NPs) morphology widely reported in the literature. A continuous layer may have less specific reactive surface areas than discrete NPs, but it avoids coarsening of the NPs and thus is expected to be morphologically more stable.[19] The first enabler for the conformal coating is the structural similarity between the two layers. The compositional analysis by STEM-EDX indicates that Ta from SCT is mostly concentrated in the outer layer, suggesting that it is likely the SCT capping layer. The diffraction patterns of **Figure 1 (c)** by TEM-SAED reveal that SCT and LSCF are virtually isostructural with identical (110) *d*-spacings (0.28 nm). This is not surprising given the fact that both SCT and LSCF are perovskites with corner-shared 3*d* metal-oxygen octahedra.[18,20] However, having the same *d*-spacing seems to suggest that cation interdiffusions between SCT and LSCF may play a role in the chemical homogenization (except for Ta).

The second enabler for the continuous coating is the high calcination temperature. Early studies have indeed shown the dependence of the morphology of an infiltrated species upon the calcination temperature. For example, Lou *et al*. reported a discrete NPs morphology when calcining the isostructural $Sm_{0.5}Sr_{0.5}O_{3-\delta}$ on a LSCF skeleton at 800 °C.[21] Similar morphologies for SCT@LSCF are also observed in the present work at 800 °C when calcined for 2 h (see **Figure S1**). At higher calcination temperatures, such as ≥1000 °C, a transitional discrete-to-continuous layer of NPs was observed in non-isostructures (perovskite/fluorite) such as (Sm, Ce)-doped $SrCoO_{3-\delta}$@$Sm_{0.2}Ce_{0.8}O_{1.9}$ at 1100 °C,[22] and $LaNi_{0.6}FeO_{3-\delta}$ @ YSZ (yttria-stabilized zirconia) at 1100 °C.[23] However, no conformally coated structure such as the SCT@LSCF observed here, has been previously reported. To facilitate the understanding of this temperature-morphology relationship, we schematically illustrate in **Figure 1 (d)** the formation of discrete NPs and the continuous layer of SCT on LSCF at low and high temperature regimes, respectively.

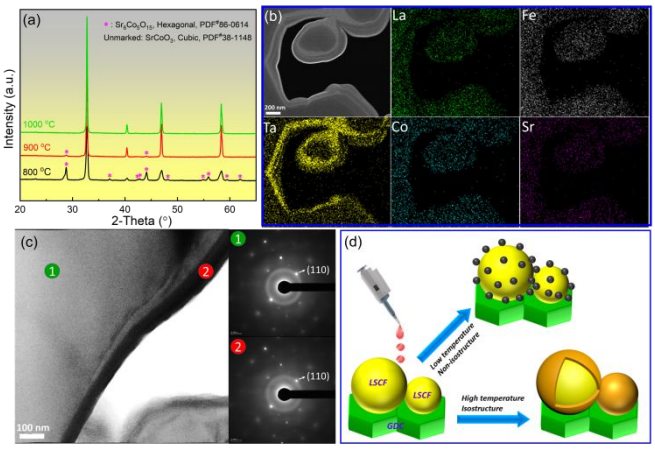

Figure 1. (a) XRD patterns of SCT vs calcination temperature; (b) STEM image/EDX mapping; and (c) TEM images/SAED patterns of the SCT@LSCF-GDC cathode after calcination at 1000 °C for 2h. Only the portion belonging to SCT@LSCF is shown here; (d) a schematic illustrating the effect of calcination temperature on morphology.

The ORR performance and Cr-tolerance of both the untreated (LSCF-GDC) and infiltrated (SCT@LSCF-GDC) cathodes are evaluated side-by-side in the same testing rig to avoid data variability. **Figure 2** shows the EIS-extracted polarization resistance (R_P) *vs* time at 700 °C for the two cathodes. The original EIS spectra can be found in **Figure S2**.

During the first 234-h of testing in clean air, the infiltrated cathode clearly outperforms the untreated one by demonstrating at least 4.5× lower R_P values. Single fuel cell testing with infiltrated cathode also shows better performance than the untreated cell (see **Figure S3**). As soon as the Cr-source (SS430) is introduced into the air stream, the untreated cathode responds with an appreciable jump in R_P, followed by a nearly monotonic increase with time. In contrast, response of the infiltrated cathodes to the Cr-addition is much less pronounced, with only a marginal increase. Compared with recent literature results tested in Cr-containing air, e. g. BaO infiltrated LSCF at 800 °C,[13] $La_2NiO_{4+\delta}$ (LNO) infiltrated $PrBa_{0.5}Sr_{0.5}Co_{1.5}Fe_{0.5}O_{5+\delta}$ (PBSCF) at 750 °C,[24] GDC infiltrated LNF at 750 °C,[25] LNF-GDC composite at 700 °C,[26] LSCF at 750 °C,[27] BSCF at 800 °C,[28] in **Figure S4** we show that SCT@LSCF-GDC at 700 °C outperforms most of those materials, even though the former are at higher temperatures. $BaCeO_3$ [29] and $PrO_x/PrNi_{0.5}Mn_{0.5}O_3$ (PNM)[27] infiltrated LSCFs show smaller R_p values than SCT@LSCF-GDC, but they are also at higher temperatures (800 and 750 °C) and are only tested for much shorter times (40 and 72 h, respectively). We show later that the better Cr-resistance and ORR activity of the new infiltrated cathode demonstrated here are fundamentally derived from its SrO-free surface and thermodynamics.

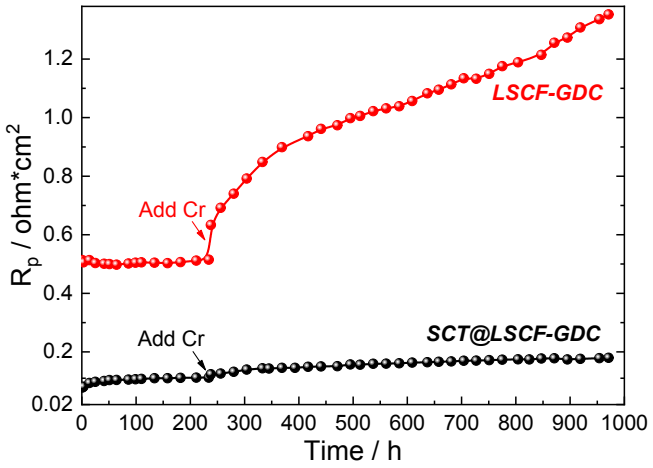

Figure 2. Time-dependent R_P of the untreated and infiltrated cathodes in clean and Cr-containing atmospheres.

Similarly, the effects of CO_2 and H_2O on R_P values of both cathodes shown in **Figure S5** indicate that the change in R_P (ΔR_P) induced by CO_2 and H_2O is far less for the infiltrated than for the untreated cathode in the temperature range of 550 to 700 °C, even though the overall impacts of these low concentrations of CO_2 and H_2O are marginal compared to the Cr-effect shown in **Figure 2**. It is also interesting to notice that the CO_2 and H_2O effects are more pronounced at low temperatures than at high temperatures, implying the physical adsorption nature (not reaction) of the effect.

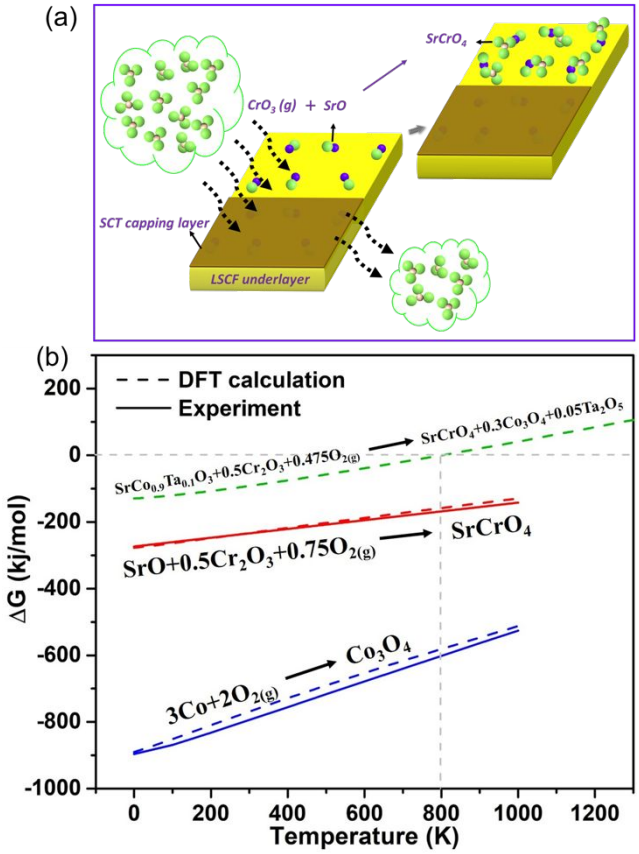

Figure 3. (a) Schematics of the untreated and infiltrated cathode illustrating why it is chemically tolerant to Cr species in air. (b) First principle DFT-based calculations of the Gibbs free energy change of Cr-involved chemical reactions.

The results presented so far clearly demonstrate the infiltrated cathode's better Cr-tolerance and superior ORR activity compared to the single-layer LSCF-GDC. To facilitate mechanistic understanding, we schematically show the surface reactions of the two cathodes in a Cr-containing environment in **Figure 3 (a)**. It should be noted that the surface Sr-segregation in LSCF is well documented in literature[30,31] and has also been confirmed in this study by our combined SEM and XPS analysis, showing a significantly higher level of surface Sr in LSCF than SCT (see **Figure S6**). In the presence of SrO on the surface of LSCF, the gaseous Cr-species such as $CrO_{3(g)}$ will readily react with SrO to form $SrCrO_4$. The formed $SrCrO_4$ is insulating and inactive, thus blocking ORR active sites. In contrast, SCT will not react with $CrO_{3(g)}$ because of its SrO-free

surface. To further support the mechanistic findings, we carried out thermodynamic calculations of the Gibbs free energy change (ΔG) of the SCT-Cr reaction. Since the formation ΔG of SCT is unknown, we applied first-principle density functional theory (DFT) to calculate ΔG of the following reaction (details can be found in the ESI):

$SrCo_{0.9}Ta_{0.1}O_3 + 0.5Cr_2O_3 + 0.475O_{2(g)} = SrCrO_4 + 0.3Co_3O_4 + 0.05Ta_2O_5$ (1)

Note that first-principle DFT calculations have been demonstrated in recent years as a useful tool to calculate thermodynamic quantities.[32,33] The calculation results in **Figure 3 (b)** indicate that SCT will not react with $CrO_{3(g)}$ (in the form of Cr_2O_3+O_2) above 800 K, while SrO is highly reactive with $CrO_{3(g)}$. In **Figure 3 (b),** to ensure the accuracy and fidelity of the calculations, we also compare ΔG calculated from DFT with the experimental data of two well-known reactions; the shown excellent agreements demonstrate that the calculations for SCT-Cr reactions are reliable.

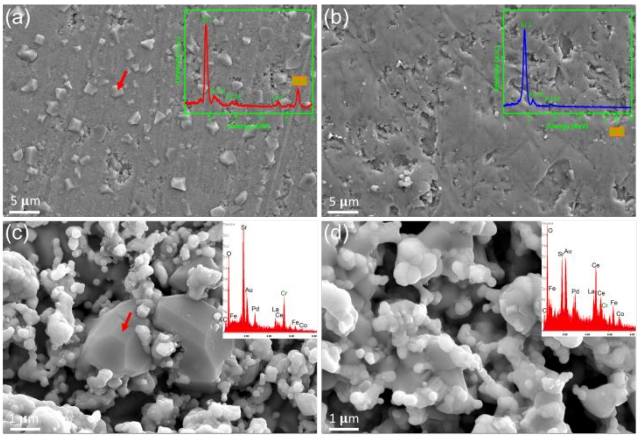

Figure 4. SEM and EDX of (a) LSCF pellets and (b) SCT pellets after annealing at 900 °C for 100 h; (c) LSCF-GDC and (d) SCT@LSCF-GDC after 1,000-h at 700 °C in Cr-rich air. The EDX was taken over the whole presented area.

The hypothesis that the surface SrO is the active site to attract Cr-species is also verified experimentally by exposing dense LSCF and SCT pellets to a Cr-containing air at 900 °C for 100 h, followed by surface analysis of SEM/EDX. For the LSCF sample, many crystalline precipitates are clearly visible in **Figure 4 (a)**. The EDX results suggest that these particles are Sr and Cr-containing compound, presumably $SrCrO_4$, even though the semi-quantitative EDX suggests a Sr/Cr >1 (some Sr may come from the LSCF base). Raman spectroscopic study (see **Figure S7**) of these particles indicates shifts at 854 cm^{-1}, 880 cm^{-1} and 899 cm^{-1}, matching well to the characteristic shifts of pure $SrCrO_4$. In contrast, the SCT surface shown in **Figure 4 (b)** is clean and no Cr is detectable from the EDX. A more direct evidence of the Cr-resistance in the infiltrated cathode is given in **Figure 4 (c)** and **(d)**, where the microstructures and local compositions of the two post-tested symmetrical cells (results in **Figure 2**) are closely examined at the cathode/electrolyte interface. The untreated LSCF-GDC sample, shown in **Figure 4 (c),** contains distinctive and large-grained Sr- and Cr-rich phases. In contrast, **Figure 3 (d)** reveals the infiltrated cathode with no apparent $SrCrO_4$ phase in the microstructure and a minimum amount of Cr detected by EDX.

In summary, a conformally coated cathode consisting of a SCT top nanoscaled layer and LSCF-GDC underlying skeleton has been demonstrated for the first time through combined solution infiltration and high temperature calcination. Owing to the excellent ORR activity and SrO-free surface in the top SCT layer, SCT@LSCF-GDC exhibits a much lower and more stable polarization resistance than its single layer LSCF-GDC counterpart. More importantly, the SrO-free surface in SCT shuts down the degradation mechanisms invoked by $CrO_{3(g)}$, H_2O or CO_2, thus making the new cathode more resilient and suited for SOFCs to operate under real-world conditions with low degradation rates.

Conflicts of interest

There are no conflicts to declare.

Acknowledgements

This work was funded by National Energy Technology Laboratory, Office of Fossil Energy, U.S. Department of Energy, under award number DE-FE-0031671.

References

1. E. D. Wachsman and K. T. Lee, *Science*, 2011, **334**, 935-939.
2. Z. Gao, L. V. Mogni, E. C. Miller, J. G. Railsback and S. A. Barnett, *Energy & Environmental Science*, 2016, **9**, 1602-1644.
3. C. Xia and M. Liu, *Solid State Ionics*, 2001, **144**, 249-255.
4. Z. Shao and S. M. Haile, in *Materials for Sustainable Energy: A Collection of Peer-Reviewed Research and Review Articles from Nature Publishing Group*, World Scientific, 2011, pp. 255-258.

5. D. Oh, D. Gostovic and E. D. Wachsman, *J. Mater. Res.*, 2012, **27**, 1992-1999.
6. W. Jung and H. L. Tuller, *Energy & Environmental Science*, 2012, **5**, 5370-5378.
7. W. Lee, J. W. Han, Y. Chen, Z. Cai and B. Yildiz, *J Am Chem Soc*, 2013, **135**, 7909-7925.
8. N. Ni, C. C. Wang, S. P. Jiang and S. J. Skinner, *Journal of Materials Chemistry A*, 2019, **7**, 9253-9262.
9. S. J. Skinner, *Adv Mater Interfaces*, 2019, 1900580.
10. Y. Zhen, A. Tok, S. P. Jiang and F. Boey, *Journal of Power Sources*, 2007, **170**, 61-66.
11. Y. Zhen and S. P. Jiang, *Journal of Power Sources*, 2008, **180**, 695-703.
12. X. Chen and S. P. Jiang, *Journal of Materials Chemistry A*, 2013, **1**, 4871-4878.
13. K. Chen, N. Ai, K. M. O'Donnell and S. P. Jiang, *Physical Chemistry Chemical Physics*, 2015, **17**, 4870-4874.
14. J. Hong, A. Aphale, S. J. Heo, B. Hu, M. Reisert, S. Belko and P. Singh, *Acs Appl Mater Inter*, 2019.
15. A. Aphale, M. A. Uddin, B. Hu, S. J. Heo, J. Hong and P. Singh, *Journal of The Electrochemical Society*, 2018, **165**, F635-F640.
16. J. A. Schuler, A. J. Schuler, D. Penner, A. Hessler-Wyser and C. Ludwig, *Electrochemical and Solid-State Letters*, 2011, **14**, B132-B134.
17. T. Yang, X. Jin and K. Huang, Journal of Membrane Science, 2018, **568**, 47-54.
18. J. Wang, T. Yang, L. Lei and K. Huang, *Journal of Materials Chemistry A*, 2017, **5**, 8989-9002.
19. Y. Gong, D. Palacio, X. Song, R. L. Patel, X. Liang, X. Zhao, J. B. Goodenough and K. Huang, *Nano letters*, 2013, **13**, 4340-4345.
20. G. Corbel, S. Mestiri and P. Lacorre, *Solid state sciences*, 2005, **7**, 1216-1224.
21. X. Lou, S. Wang, Z. Liu, L. Yang and M. Liu, *Solid State Ionics*, 2009, **180**, 1285-1289.
22. D. Chen, G. Yang, F. Ciucci, M. O. Tadé and Z. Shao, *Journal of Materials Chemistry A*, 2014, **2**, 1284-1293.
23. S. Lee, M. Bevilacqua, P. Fornasiero, J. Vohs and R. Gorte, *Journal of Power Sources*, 2009, **193**, 747-753.
24. J. Li, J. Li, D. Yan, J. Pu, B. Chi and L. Jian, *Electrochimica Acta*, 2018, **270**, 294-301.
25. B. Huang, X.-j. Zhu, R.-x. Ren, Y.-x. Hu, X.-y. Ding, Y.-b. Liu and Z.-y. Liu, *Journal of Power Sources*, 2012, **216**, 89-98.
26. Y. Ling, H. Xie, Z. Liu, X. Du, H. Chen, X. Ou, L. Zhao and R. A. Budiman, *Electronic Materials Letters*, 2018, **14**, 432-439.
27. Y. Chen, S. Yoo, X. Li, D. Ding, K. Pei, D. Chen, Y. Ding, B. Zhao, R. Murphy and B. Deglee, *Nano Energy*, 2018, **47**, 474-480.
28. Y.-M. Kim, X. Chen, S. P. Jiang and J. Bae, *Electrochemical and Solid-State Letters*, 2011, **14**, B41-B45.
29. K. Chen, M. Li, N. Ai and S. P. Jiang, Meeting Abstracts, *The Electrochemical Society*, 2016, 2881-2881.
30. P. Van Der Heide, *Surface and Interface Analysis: An International Journal devoted to the development and application of techniques for the analysis of surfaces, interfaces and thin films*, 2002, **33**, 414-425.
31. E. J. Crumlin, E. Mutoro, Z. Liu, M. E. Grass, M. D. Biegalski, Y.-L. Lee, D. Morgan, H. M. Christen, H. Bluhm and Y. Shao-Horn, *Energy & Environmental Science*, 2012, **5**, 6081-6088.
32. F. Calle‐Vallejo, J. I. Martínez, J. M. García‐Lastra, M. Mogensen and J. Rossmeisl, *Angewandte Chemie International Edition*, 2010, **49**, 7699-7701.
33. L. Wang, T. Maxisch and G. Ceder, *Physical Review B*, 2006, **73**, 195107.

TOC

SCT conformally coated LSCF-GDC cathode shows significantly improved ORR activity with a strong Cr-tolerance.